Photocatalytic Hydrogen Generation from a Visible-Light Responsive Metal-Organic Framework System: The Impact of Nickel Phosphide Nanoparticles

*Stavroula Kampouri,[a] Tu N. Nguyen,[a] Christopher P. Ireland,[a] Bardiya Valizadeh,[a] Fatmah Mish Ebrahim,[a] Gloria Capano,[a] Daniele Ongari,[a] Amber Mace,[ab] Nestor Guijarro Carratala,[c] Kevin Sivula,[c] Andrzej Sienkiewicz,[d] László Forró,[d] Berend Smit,[a] Kyriakos C. Stylianou[a]**

[a.] Institute of Chemical Sciences and Engineering (ISIC), Ecole Polytechnique Fédérale de Lausanne (EPFL Valais), Rue de l'industrie 17, 1951 Sion (Switzerland). E-mail: Kyriakos.stylianou@epfl.ch

[b.] Department of Materials and Environmental Chemistry, Arrhenius Laboratory Stockholm University.

[c.] Institute of Chemical Sciences and Engineering (ISIC), Ecole Polytechnique Fédérale de Lausanne (EPFL), Station 6, 1015 Lausanne (Switzerland).

[d.] Institute of Physics, Ecole Polytechnique Fédérale de Lausanne (EPFL), Station 3, 1015 Lausanne (Switzerland).

† Electronic Supplementary Information (ESI) available: Experimental methods, Synthetic procedures, characterization and computational details. This material is available free of charge via the internet at See DOI: 10.1039/x0xx00000x

Abstract: Herein, we report the performance of a photocatalytic system based on the visible-light active MIL-125-NH_2 mixed with nickel phosphide (Ni_2P) nanoparticles. This combination boosts the H_2 evolution rate to an outstanding value of 894 μmol h^{-1} g^{-1} under visible-light irradiation, which is among the highest H_2 evolution rates reported to date for metal-organic frameworks (MOFs). The H_2 generation rate produced by Ni_2P/MIL-125-NH_2 is almost 3 times higher than that of Pt/MIL-125-NH_2 system, highlighting the impact of the co-catalyst in photocatalytic water splitting. Additionally, our system outperforms the Ni_2P/TiO_2 system under UV-Vis irradiation. The exceptional performance of Ni_2P/MIL-125-NH_2 is due to the efficient transfer of photogenerated electrons from MIL-125-NH_2 to Ni_2P, high intrinsic activity of Ni_2P and exceptional synergy between them. This system exhibits the highest apparent quantum yields of 27.0 and 6.6 % at 400 and 450 nm, respectively, ever reported for MOFs.

Hydrogen (H_2) gas is widely produced and used in industries, particularly in fossil fuel processing and ammonia synthesis.[1] In addition, it is considered as a clean energy carrier for a sustainable energy future, since the combustion of H_2 results in the generation of water and no greenhouse gasses, which eliminates the risk of climate change and allows for a carbon-neutral energy cycle.[2] Traditional methods for H_2 production include methane steam reforming and coal gasification; however, these processes also produce carbon dioxide as a by-product that needs to be captured and sequestered.[3] H_2 can also be generated from water electrolysis using electricity but the electricity must also be obtained from a renewable energy source such as solar, wind, hydroelectric, or hydrothermal energy. A superior method to generate H_2 is through artificial photosynthesis, which utilizes the inexhaustible solar energy to directly convert water into H_2.[4] Owing to the sustainable nature of this procedure and the potential cost efficiency, many research efforts in materials science have been focused on developing novel photocatalytic systems that can enhance the rate of H_2 evolution, with 10% quantum efficiencies being the lower limit for commercial applications to be feasible.[5,6] However, due to the negligible absorptivity of traditional photocatalysts such as TiO_2 and SnO_2 toward the visible-light, the low water stability of other alternatives such as CdS or GaAs, and the high cost of noble metal co-catalysts, no photocatalytic systems have been industrially applied.[7,8]

A metal-organic framework (MOF) is a network of metal ions or clusters bridged by organic ligands through coordination bonds into a porous extended structure.[9-11] MOFs offer the exciting possibility to integrate a light harvesting moiety (ligand), a catalytic component (reductive metal ions), and intrinsic porosity into a single structure.[12,13] Therefore, the utilization of MOFs can be a pioneering key for the field of photocatalytic H_2 generation.[14-16] A MOF-based photocatalytic system can consist of several components in addition to the MOF, which is the main component and usually acts as an antenna harvesting light. Upon illumination, the MOF generates charge-carriers (electrons and holes) with the electrons being responsible to reduce H_2O into H_2. In addition to the MOF photocatalyst, the photocatalytic system (for H_2 generation) usually comprises: *i.* a co-catalyst that can attract the photogenerated electrons; *ii.* a photosensitizer that may be used to extend the light absorption into the visible region, when a UV-light-active (MOF) photocatalyst is used;[17] *iii.* a sacrificial agent that is usually employed as an electron donor to scavenge the photogenerated holes; and *iv.* a redox shuttle which can expedite the charge transfer between the photocatalyst and the co-catalyst.[18]

Several MOF-based photocatalytic systems have been tested for visible-light driven H_2 production; most of them are based on reductive metal ions such as Ti^{IV} and Zr^{IV} and visible-light-active ligands that can harvest solar light and convert it into H_2 (Tables 1 and S2).[17-29] Recently, Cu^{I} or Cu^{II}-based MOFs were found to be good candidates to photocatalytically reduce H_2O into for H_2 under UV/vis or visible irradiation (Table S2).[30-32] Despite the high promise of MOFs towards water splitting, the majority of these MOF-based systems demonstrate very low apparent quantum yields or still utilize expensive noble-metal co-catalysts such as Pt nanoparticles (NPs).[18,20] The latter is due to the easy preparation and intrinsic activity of Pt NPs, yet their use does not guarantee the best photocatalytic performance. Although very few examples have been reported in the literature, the synergy between MOFs and co-catalysts is proven to be a key factor for the photocatalytic performance of the system, as different hydrogen generation rates and quantum yields are observed when the same MOF is used (Tables 1). Consequently, there is a need to investigate the activity of alternative co-catalysts and identify photocatalytic systems and conditions optimum for water splitting and hydrogen generation.

Table 1: Comparison of the visible-light driven photocatalytic performance of systems utilizing MIL-125-NH_2 as the photocatalyst with different co-catalysts.

Co-catalyst	Light Source λ (nm)	HER_P (μmol h^{-1} g^{-1})	Apparent Quantum Yield (%)	Stability (h)	Ref.
Pt NPs	≥ 420	*333	-	> 9	15
Pt NPs	≥ 420	*525	-	> 9	16
Co^{II} complex	≥ 380	553	-	> 7.5	17
Co^{III} oxime	≥ 408	*637	0.5	> 70	18
Ni_2P NPs	**≥ 420**	**894**	**6.6-450nm 27.0-400nm**	**> 84**	**This work**

HER_P: H_2 evolution rate with respect to the photocatalyst

* Calculated based on reported data

Herein, we report a photocatalytic system consisting of the visible-light absorbing MIL-125-NH_2 as the photocatalyst and the Ni_2P nanoparticles (NPs) as the co-catalyst. Although both materials have been tested with other photocatalysts or co-catalysts,[23,33] our Ni_2P/MIL-125-NH_2 system exhibits H_2 evolution rates and apparent quantum yields (AQY) under visible-light

irradiation, that are among the highest values reported to date for MOFs. The H_2 generation rate produced by Ni_2P/MIL-125-NH_2 is almost 3 times higher than the Pt/MIL-125-NH_2 system tested under the same reaction conditions, suggesting that the selection of the co-catalyst is crucial for the design of efficient photocatalytic systems. In addition, Ni_2P/MIL-125-NH_2 outperforms Ni_2P/TiO_2, with TiO_2 being the most well studied photocatalyst for water splitting,[34] highlighting the exceptional synergy between MIL-125-NH_2 and Ni_2P.

MIL-125-NH_2 and Ni_2P NPs were synthesized and characterized according to reported procedures (Sections S1-S7).[23,35] The size of the NPs is around 16-19 nm as shown by Transmission Electron Microscopy (TEM) images, and the N_2 isotherm collected at 77 K revealed a BET surface area of 27.8 m^2/g (Fig. S2-S5). In order to assess the performance and optimize the composition of our photocatalytic system toward H_2 generation, different combinations of MIL-125-NH_2 and Ni_2P powders were mixed in a reactor containing a solvent mixture of acetonitrile (CH_3CN), triethylamine (TEA) as the sacrificial agent, and water. The reactor was then irradiated with visible light by a 300 W Xe lamp using a long-pass cut-off filter allowing $\lambda \geq 420$ nm, and the generated H_2 was analysed by gas chromatography. As shown in Fig. S7 and S8, when increasing amounts of Ni_2P were added to a constant amount of MIL-125-NH_2, the H_2 evolution rate increases since the co-catalyst attracts the electrons efficiently, inhibiting the undesired charge carrier recombination. By reaching 9.2 (± 0.4) wt% of Ni_2P, the H_2 evolution rate is maximized. At this ratio, there is an optimum level of interactions between Ni_2P and MIL-125-NH_2, promoting the electron transfer to the Ni_2P. Further increasing the amount of Ni_2P leads to a decrease in the H_2 production rate, as the interaction between MIL-125-NH_2 and the Ni_2P is already at its maximum, while the Ni_2P NPs simultaneously compete with MIL-125-NH_2 in light absorption, shielding-effect.[36] As displayed in Fig. S9, the Ni_2P/MIL-125-NH_2 system exhibits a highly enhanced activity that is almost 300 times higher than that of the pristine MIL-125-NH_2 (2.249 μmol h^{-1} g^{-1}), reaching a H_2 evolution rate of 648 μmol $h^{-1}g^{-1}$ and 7865 μmol $h^{-1}g^{-1}$ with respect to MIL-125-NH_2 and Ni_2P. Blank photocatalytic experiments (under visible-light irradiation) using solely Ni_2P with and without the NH_2-H_2BDC (amino-terephthalic acid) ligand resulted in no H_2 generation, confirming the unique advantage of having MIL-125-NH_2 as a photocatalyst within the system. Moreover, recycling experiments for the optimum ratio between Ni_2P and MIL-125-NH_2 revealed that the H_2 evolution rate of this system remains stable for at least seven catalytic runs (each for 12 h, Fig. S10). The PXRD patterns of the samples before and after photocatalysis are comparable, confirming that the crystallinity of both MIL-125-NH_2 and Ni_2P is retained after 84 h of continuous irradiation (Fig. S10).

We further examined the performance of Ni_2P/MIL-125-NH_2 by varying the solvent mixtures; we kept the same ratio of acetonitrile and TEA, whereas the H_2O content was varied from 1.63 v/v% to 8.19 v/v% (V_{total} was kept constant) (Fig. 1a and S11). By increasing the water content, the H_2 evolution rate also increases. With the optimum photocatalytic solution of 4.87 v/v% water, the photocatalytic system reached a H_2 evolution rate of 894 μmol h^{-1} g^{-1} and 10134 μmol h^{-1} g^{-1} with respect to the MIL-125-NH_2 and Ni_2P. To the best of our knowledge, this is among the highest H_2 evolution rate for a visible-light active photocatalytic-MOF system reported to date (Table 1).[19,20,23]. The AQYs of the optimum system at 400 and 450 nm were calculated by Ferrioxalate actinometry [37,38] and reached values of 27.0 and 6.6 %, respectively (Section S9). These are the highest reported efficiencies for MOFs[18,23,39] (Tables 1 and S2) and comparable to leading photocatalysts.[40,41]

In order to compare our photocatalytic MOF system with TiO_2, we investigated the parallel photocatalytic performance of Ni_2P/MIL-125-NH_2 and Ni_2P/TiO_2 toward H_2 generation, under irradiations that include UV light since TiO_2 is characterized by an overly large optical band gap (~3 eV) and operates only under UV irradiation. Commercial TiO_2 (P25, Degausa - which is a standard material in the field of TiO_2-photocatalyzed reactions) was used[42] and the amount of Ni_2P added was

first varied in order to determine the optimum system. In order to compare our photocatalytic MOF system with TiO_2, we investigated the parallel photocatalytic performance of Ni_2P/MIL-125-NH_2 and Ni_2P/TiO_2 toward H_2 generation, under irradiations that include UV light since TiO_2 is characterized by an overly large optical band gap (~3 eV) and operates only under UV irradiation. The optimum Ni_2P/TiO_2 system contains 15.3 (± 0.4) wt% of Ni_2P (Section S10). The best performing Ni_2P/MIL-125-NH_2 and Ni_2P/TiO_2 systems generated H_2 with a rate of 3878 and 1708 μmols g^{-1} h^{-1}, with respect to the MIL-125-NH_2 and TiO_2, and the AQY for Ni_2P/TiO_2 at 400 nm was found to be 0.9 % (Fig. 1b and Section S9). It is apparent that by a simple subtraction of the visible-light-driven H_2 evolution rate previously obtained (894 μmol h^{-1} g^{-1}), Ni_2P/MIL-125-NH_2 outperforms Ni_2P/TiO_2 even in the UV light region. This can be attributed to the high porosity of MIL-125-NH_2 (BET: 1197.5 m^2/g) that allows for easy light penetration compared to the solid TiO_2, the high molar absorptivity of MIL-125-NH_2, and particularly the exceptional synergy between MIL-125-NH_2 and Ni_2P.

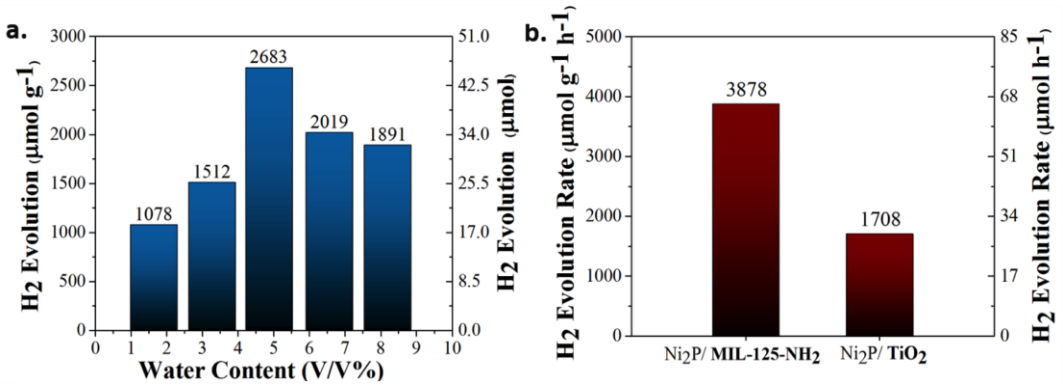

Fig. 1 (a) H_2 evolution of the optimum Ni_2P/MIL-125-NH_2 system with different water contents under visible-light irradiation for 3 hours and (b) Maximum H_2 evolution rates of 9.2 (±0.4) wt% Ni_2P/MIL-125-NH_2 and 15.3 (± 0.4) wt% Ni_2P/TiO_2 with respect to the photocatalyst under UV/vis light irradiation for 3 hours.

As indicated in previous studies, the NH_2-BDC within MIL-125-NH_2 acts as an antenna that absorbs light and promotes an electron from the Highest Occupied Crystalline Orbitals (HOCOs) to the Lowest Unoccupied Crystalline Orbitals (LUCOs) of MIL-125-NH_2. The HOCOs comprise mainly the π orbitals of the ligand while the LUCOs have contributions from the O 2p and the Ti 3d orbitals.[43,44] As proposed by Santaclara *et al.*, upon illumination, electron-hole pairs are generated, with the holes mainly localized and restricted in movement in the -NH_2 groups of the ligand, whereas the electrons are relatively free to migrate to the Ti 3d orbitals (confirmed by the presence of Ti^{3+} in the electron paramagnetic resonance (EPR) spectrum of MIL-125-NH_2 shown in Fig. 2), thus allowing effective charge separation.[42,45] Such charge separation provides an efficient stabilization of the photoexcited species; a key element for allowing the electrons to reach the surface of MIL-125-NH_2, before their recombination with the holes.

In order to further understand the localization of the charge-carriers, our density functional theory (DFT) calculations showed that after injection of a single hole and a single electron, the hole is localized in the πorbital of NH_2-BDC whereas the electron is not only localized on the Ti 3d orbitals but also delocalized along the NH_2-BDC ligand. The delocalized states of electrons ensure their efficient transfer to the surface of MIL-125-NH_2 (Section S11). Subsequently, in our photocatalytic system, the photo-excited electron is transferred from the LUCOs of MIL-125-NH_2 to Ni_2P, as evidenced by the presence of Ni^+ in the EPR spectrum of Ni_2P/MIL-125-NH_2 (Fig. 2 and Section S12), and then to the protons. Inductively couple plasma optical emission spectrometry (ICP-OES) studies (Section S13) and SEM mapping images of the Ni_2P/MIL-125-NH_2 (Fig. S12, S13) reveal that 90 % of Ni_2P NPs are attached and evenly distributed on the external surface of MIL-125-NH_2 crystals suggesting that efficient electron transfer

can occur. In terms of thermodynamics of electron transfer, from the energy diagram (Fig. S22), the conduction band of Ni_2P has a lower reduction potential ($E_{vac.}$= -4.50 eV)[46] than the LUCOs of MIL-125-NH_2 ($E_{vac.}$= -3.80 eV), and is in the same level as the reduction potential of H^+/H_2 ($E_{vac.}$= -4.50 eV, E_{NHE}= 0 eV).[43] This large negative energy difference between MIL-125-NH_2 and Ni_2P stems from the discrete Ti_8O_8 cluster on MIL-125-NH_2 being exceptionally reducing. This contrasts with TiO_2 in which the extended structure conduction band is at the lower reduction potential of -4.25 eV, compared to the discrete cluster. Consequently, in TiO_2, the lower reduction potential negates the reductive power of TiO_2 compared to MIL-125-NH_2, and therefore, decreases the effectiveness of the electron transfer to the Ni_2P.[47] The smaller thermodynamic driving force confirms the lower performance of Ni_2P/TiO_2.

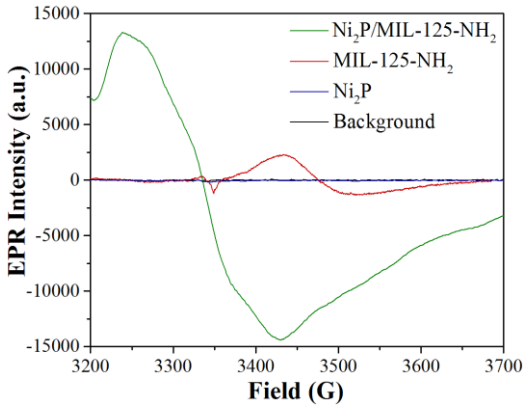

Fig. 2 EPR spectra of 9.2 (±0.4) wt% Ni_2P/MIL-125-NH_2 (green), MIL-125-NH_2 (red), Ni_2P (blue) after visible light irradiation.

Insights into the catalytic activity of Ni_2P can be obtained by comparing Ni_2P/MIL-125-NH_2 with other systems. Nasalevich *et al.* reported a system containing cobaloxime complexes encapsulated within the pores of MIL-125-NH_2 in MeCN/TEA/H_2O mixture. This system produces H_2 with a maximum rate of 637 μmol g^{-1} h^{-1}. Since the cobaloxime complex ($E_{vac.}$= -4.25 eV) has a higher reduction potential than that of Ni_2P (but lower than the LUCOs of MIL-125-NH_2), the energy difference is less, which is a key reason for its inferior performance compared to Ni_2P/MIL-125-NH_2 (Fig. S23).[23] Matsuoka *et al.* reported that the Pt/MIL-125-NH_2 system in 0.01 M aqueous TEOA solution displays a maximum H_2 evolution rate of 525 μmol g^{-1} h^{-1}.[20] Upon testing Ni_2P/MIL-125-NH_2 in 0.01 M TEOA aqueous solution, we observed that the photocatalytic solution darkened and the MIL-125-NH_2 degraded and dissolved (Section S14.1).

In order to compare the performance of Ni_2P/MIL-125-NH_2 with Pt/MIL-125-NH_2, we synthesized "naked" Pt NPs[48] with the size of ~19 nm (Fig. S28, S29). We then mixed them with MIL-125-NH_2 and investigated the performance of this system using the same conditions used for Ni_2P/MIL-125-NH_2. The Pt/MIL-125-NH_2 produced H_2 with a maximum evolution rate of 269 μmol g^{-1} h^{-1} (Fig. S30). Based on the energy diagram shown in Fig. S23, Pt might have higher driving force compared to Ni_2P for attracting the photogenerated electrons from the MOF; however, not all electrons transferred from MIL-125-NH_2 to Pt have enough energy for the reduction of protons from H^+ to H_2. In addition, photochemical chronoamperometry measurements (Fig. 3a, S33, S34) showed that upon illumination both Ni_2P/MIL-125-NH_2 and Pt/MIL-125-NH_2 exhibit comparable initial photocurrents at the early stage, but the photocurrent in the presence of Pt NPs decays faster over time. This suggests the faster charge recombination in Pt/MIL-125-NH_2 compared to Ni_2P/MIL-125-NH_2, inhibiting thus its H_2 production performance.

The effectiveness of charge separation in the Ni_2P/MIL- 125-NH_2 and Pt/MIL-125-NH_2 was further studied by photoluminescence (PL) emission spectroscopy (Fig. 3b and S33). The suspension of MIL-125-NH_2 exhibits fluorescence with the maximum peak centered at ~560 nm when excited at 420 nm. The addition of the co-catalysts (Pt and Ni_2P NPs) diminishes the PL emission, indicating the electron transfer from MIL-125-NH_2 to the co-catalysts and depopulating the excited electrons in MIL-125-NH_2. However, in the case of Ni_2P/MIL-125-NH_2, the quenching of the photoluminescence is more drastic and when the amount of Ni_2P reaches 9.2 (± 0.4) wt% (optimum amount), the mixture Ni_2P/MIL-125-NH_2 shows no detectable photoluminescence emission, illustrating the key role of these NPs in attracting the electrons and thus eliminating the electron-hole recombination. On the other hand, the addition of the 2.0 (± 0.4) wt% amount of Pt (optimized Pt/MIL-125-NH_2 system), does not induce complete quenching of the PL emission. Lifetime measurements of MIL-125-NH_2, and the optimized Pt/ MIL-125-NH_2 and Ni_2P/MIL-125-NH_2 systems revealed that the latter has shorter lifetime compared to the others (Fig. 3c), confirming the more efficient electron transfer from MIL-125-NH_2 to Ni_2P.

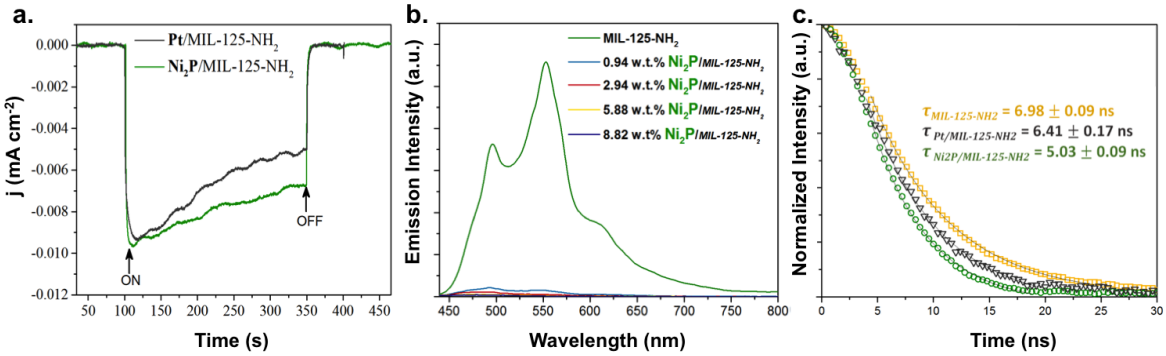

Fig. 3 (a) Photocurrent responses of MIL-125-NH_2 with the optimized amounts of co-catalysts (Ni_2P green and Pt black), (b) PL spectra (excited at 420 nm) for the suspensions of MIL-125-NH_2 with different amounts of Ni_2P and (c) Time Resolved PL decay curves of MIL-125-NH_2 (yellow squares), Pt/MIL-125-NH_2 (grey triangles) and Ni_2P/MIL-125-NH_2 (green circles). The excitation wavelength was 420 nm.

While it is not straightforward to compare the catalytic activity of Pt and Ni_2P, it is apparent that a good co-catalyst should be able to trap protons, transfer electrons, bond the hydrogen atoms, and desorb the H_2 molecules formed. Ni_2P NPs, with the presence of both Ni and P sites on their surface of the NPs acting as hydride and proton-acceptor centers exhibit particularly good behaviour for H_2 generation when combined with MIL-125-NH_2.[49] [50] These results highlight the impact of the co-catalyst in enhancing the performance of a photocatalytic MOF based system.[51]

Conclusions

In conclusion, we report a low-cost, stable, and easily prepared (based on mixing) photocatalytic system consisting of MIL-125-NH_2 and Ni_2P NPs that exhibits remarkable H_2 generation. The system appreciably outperforms Ni_2P/TiO_2 under UV irradiation and other visible-light active MOF systems, while maintaining its integrity for a long time. The absorptivity in the visible region, the charge separation in MIL-125-NH_2, the efficient electron transport to the external surface of MIL-125-NH_2 *via* a delocalized state, the efficient attraction of electrons by the Ni_2P NPs (compared to Pt NPs) and the inherent nature of Ni_2P to catalyze the H_2 generation are the key factors for the significantly enhanced photocatalytic activity of this system. With high apparent quantum yields under visible-light irradiation and easy scale-up synthesis of both MIL-125-NH_2 and Ni_2P NPs, this photocatalytic system brings itself a step closer to practical 'solar-driven' applications.

Conflicts of interest

KCS, BS, SK, CPI, TNN and EPFL have filed a patent application (EP17180055.0) that relates to visible-light active Ti-MOFs and cheap co-catalysts for photocatalytic water splitting and hydrogen generation.

Author Contribution

SK, TNN, CPI, BV and FME have performed and analysed all experiments described in the manuscript. GC, DO, AM and BS have performed the computational studies and analysed the data. NGC and KS have carried out the photocurrent experiments and AS and LF have designed, performed and analysed the EPR experiments. KCS led the project and KCS, SK, TNN and CPI wrote the article with contributions from all co-authors.

Acknowledgements

SK, TNN and KCS thank Swiss National Science Foundation (SNF) for funding under the Ambizione Energy Grant n.PZENP2_166888. CPI is grateful to the EU for a Marie Curie Fellowship (705861 – ASPAir, H2020-MSCA-IF-2015). GC is supported by the National Center of Competence in Research (NCCR), Materials' Revolution: Computational Design and Dis-covery of Novel Materials (MARVEL), of the Swiss National Science Foundation (SNSF). The research of DO is supported by the European Research Council (ERC) under the European Union's Horizon 2020 research and innovation program (Grant Agreement No. 666983, MaGic). AM thanks the Swedish Research Council (VR) for funding.

Notes and references

(1) Ramachandran, R.; Menon, R. K. *International Journal of Hydrogen Energy* **1998**, *23*, 593.
(2) Schoedel, A.; Ji, Z.; Yaghi, O. M. *Nat Energy* **2016**, *1*.
(3) Chaubey, R.; Sahu, S.; James, O. O.; Maity, S. *RENEW. SUST. ENERG. REV.* **2013**, *23*, 443.
(4) Lewis, N. S.; Nocera, D. G. *Proceedings of the National Academy of Sciences* **2006**, *103*, 15729.
(5) Osterloh, F. E. *Chem. Mater.* **2008**, *20*, 35.
(6) Mills, A.; Le Hunte, S. *J. Photochem. Photobiol. A* **1997**, *108*, 1.
(7) Gao, W.-Z.; Xu, Y.; Chen, Y.; Fu, W.-F. *Chem. Commun.* **2015**, *51*, 13217.
(8) Sun, Z.; Zheng, H.; Li, J.; Du, P. *Energy & Environmental Science* **2015**, *8*, 2668.
(9) Rowsell, J. L. C.; Yaghi, O. M. *Microporous and Mesoporous Materials* **2004**, *73*, 3.
(10) Li, B.; Wen, H.-M.; Cui, Y.; Zhou, W.; Qian, G.; Chen, B. *Advanced Materials* **2016**, *28*, 8819.
(11) Nelson, A. P.; Farha, O. K.; Mulfort, K. L.; Hupp, J. T. *Journal of the American Chemical Society* **2009**, *131*, 458.
(12) Wang, S.; Wang, X. *Small* **2015**, *11*, 3097.
(13) Yu, X. C., Seth M. *J. Am. Chem. Soc.* **2016,**, *138*, 12320.
(14) Zhang, T.; Lin, W. *Chem. Soc. Rev.* **2014**, *43*, 5982.
(15) Wang, J.-L.; Wang, C.; Lin, W. *ACS Catalysis* **2012**, *2*, 2630.
(16) Pullen, S.; Ott, S. *Topics in Catalysis* **2016**, *59*, 1712.
(17) He, J.; Wang, J.; Chen, Y.; Zhang, J.; Duan, D.; Wang, Y.; Yan, Z. *Chemical Communications* **2014**, *50*, 7063.
(18) Fateeva, A.; Chater, P. A.; Ireland, C. P.; Tahir, A. A.; Khimyak, Y. Z.; Wiper, P. V.; Darwent, J. R.; Rosseinsky, M. J. *Angew. Chem. Int. Ed.* **2012**, *51*, 7440.

(19) Meyer, K.; Bashir, S.; Llorca, J.; Idriss, H.; Ranocchiari, M.; van Bokhoven, J. A. *Chem. Eur. J.* **2016**, *22*, 13894.
(20) Horiuchi, Y.; Toyao, T.; Saito, M.; Mochizuki, K.; Iwata, M.; Higashimura, H.; Anpo, M.; Matsuoka, M. *J. Phys. Chem. C* **2012**, *116*, 20848.
(21) Toyao, T.; Saito, M.; Horiuchi, Y.; Mochizuki, K.; Iwata, M.; Higashimura, H.; Matsuoka, M. *Catal. Sci. Technol.* **2013**, *3*, 2092.
(22) Wang, D.; Song, Y.; Cai, J.; Wu, L.; Li, Z. *New Journal of Chemistry* **2016**, *40*, 9170.
(23) Nasalevich, M. A.; Becker, R.; Ramos-Fernandez, E. V.; Castellanos, S.; Veber, S. L.; Fedin, M. V.; Kapteijn, F.; Reek, J. N. H.; van der Vlugt, J. I.; Gascon, J. *Energy Environ. Sci.* **2015**, *8*, 364.
(24) Gomes Silva, C.; Luz, I.; Llabrés i Xamena, F. X.; Corma, A.; García, H. *Chem. Eur. J.* **2010**, *16*, 11133.
(25) Wang, C.; deKrafft, K. E.; Lin, W. *J. Am. Chem. Soc.* **2012**, *134*, 7211.
(26) Zhou, J.-J.; Wang, R.; Liu, X.-L.; Peng, F.-M.; Li, C.-H.; Teng, F.; Yuan, Y.-P. *Appl. Surf. Sci.* **2015**, *346*, 278.
(27) Xiao, J.-D.; Shang, Q.; Xiong, Y.; Zhang, Q.; Luo, Y.; Yu, S.-H.; Jiang, H.-L. *Angew. Chem.* **2016**, *128*, 9535.
(28) Toyao, T.; Saito, M.; Dohshi, S.; Mochizuki, K.; Iwata, M.; Higashimura, H.; Horiuchi, Y.; Matsuoka, M. *Chem. Commun.* **2014**, *50*, 6779.
(29) Sun, X.; Yu, Q.; Zhang, F.; Wei, J.; Yang, P. *Catalysis Science & Technology* **2016**, *6*, 3840.
(30) Shi, D.; Zheng, R.; Sun, M.-J.; Cao, X.; Sun, C.-X.; Cui, C.-J.; Liu, C.-S.; Zhao, J.; Du, M. *Angewandte Chemie International Edition* **2017**, *56*, 14637.
(31) Wu, Z.-L.; Wang, C.-H.; Zhao, B.; Dong, J.; Lu, F.; Wang, W.-H.; Wang, W.-C.; Wu, G.-J.; Cui, J.-Z.; Cheng, P. *Angewandte Chemie International Edition* **2016**, *55*, 4938.
(32) Dong, X.-Y.; Zhang, M.; Pei, R.-B.; Wang, Q.; Wei, D.-H.; Zang, S.-Q.; Fan, Y.-T.; Mak, T. C. W. *Angew. Chem. Int. Ed.* **2016**, *55*, 2073.
(33) Cao, S.; Chen, Y.; Wang, C.-J.; He, P.; Fu, W.-F. *Chemical Communications* **2014**, *50*, 10427.
(34) Ohno, T.; Sarukawa, K.; Tokieda, K.; Matsumura, M. *J. Catal.* **2001**, *203*, 82.
(35) Kumar, D. P.; Choi, J.; Hong, S.; Reddy, D. A.; Lee, S.; Kim, T. K. *ACS Sustain. Chem. Eng.* **2016**, *4*, 7158.
(36) Ran, J.; Zhang, J.; Yu, J.; Jaroniec, M.; Qiao, S. Z. *Chem. Soc. Rev.* **2014**, *43*, 7787.
(37) Kuhn, H. B., S.; Schmidt, R. *Pure and Applied Chemistry* **2004**, *76.*, 2105.
(38) Hatchard, C. P., C. A. *In Proceedings of the Royal Society of London A: Mathematical, Physical and Engineering Sciences; The Royal Society: 1956* **1956**, *235*, 518.
(39) Shen, L.; Luo, M.; Liu, Y.; Liang, R.; Jing, F.; Wu, L. *Applied Catalysis B: Environmental* **2015**, *166*, 445.
(40) Maeda, K.; Teramura, K.; Lu, D.; Takata, T.; Saito, N.; Inoue, Y.; Domen, K. *Nature* **2006**, *440*, 295.
(41) Chen, X.; Shen, S.; Guo, L.; Mao, S. S. *Chem. Rev.* **2010**, *110*, 6503.
(42) Nasalevich, M. A.; Hendon, C. H.; Santaclara, J. G.; Svane, K.; van der Linden, B.; Veber, S. L.; Fedin, M. V.; Houtepen, A. J.; van der Veen, M. A.; Kapteijn, F.; Walsh, A.; Gascon, J. **2016**, *6*, 23676.
(43) Hendon, C. H.; Tiana, D.; Fontecave, M.; Sanchez, C.; D'arras, L.; Sassoye, C.; Rozes, L.; Mellot-Draznieks, C.; Walsh, A. *J. Am. Chem. Soc.* **2013**, *135*, 10942.
(44) Walsh, A.; Catlow, C. R. A. *ChemPhysChem* **2010**, *11*, 2341.
(45) Santaclara, J. G.; Nasalevich, M. A.; Castellanos, S.; Evers, W. H.; Spoor, F. C. M.; Rock, K.; Siebbeles, L. D. A.; Kapteijn, F.; Grozema, F.; Houtepen, A.; Gascon, J.; Hunger, J.; van der Veen, M. A. *Chem. Sus. Chem.* **2016**, *9*, 388.
(46) Sharon, M.; Tamizhmani, G.; Levy-Clement, C.; Rioux, J. *Solar Cells* **1989**, *26*, 303.

(47) Xu, Y.; Schoonen, M. A. A. *American Mineralogist* **2000**, *85*, 543.
(48) Zhang, B.; Xue, Y.; Sun, H.; Jiang, A.; Li, Z.; Hao, J. *RSC Advances* **2016**, *6*, 56083.
(49) Zou, X.; Zhang, Y. *Chem. Soc. Rev.* **2015**, *44*, 5148.
(50) Liu, P.; Rodriguez, J. A. *Journal of the American Chemical Society* **2005**, *127*, 14871.
(51) Chen, Y.; Qin, Z. *Catalysis Science & Technology* **2016**, *6*, 8212.